White Rose Research Online

eprints@whiterose.ac.uk
https://eprints.whiterose.ac.uk
Universities of Leeds, Sheffield and York

Deposited via The University of Leeds.

White Rose Research Online URL for this paper:
https://eprints.whiterose.ac.uk/id/eprint/236826/

Version: Accepted Version

Article:

Tong, Y., Fan, C., Fu, Z. et al. (2026) Flame impingement to facilitate the stability of NH3-CH4 laminar diffusion flames: High-speed imaging and schlieren visualization. Fuel, 414. 138297. ISSN: 0016-2361

https://doi.org/10.1016/j.fuel.2026.138297

This is an author produced version of an article published in Fuel, made available via the University of Leeds Research Outputs Policy under the terms of the Creative Commons Attribution License (CC-BY), which permits unrestricted use, distribution and reproduction in any medium, provided the original work is properly cited.

Reuse

This article is distributed under the terms of the Creative Commons Attribution (CC BY) licence. This licence allows you to distribute, remix, tweak, and build upon the work, even commercially, as long as you credit the authors for the original work. More information and the full terms of the licence here: https://creativecommons.org/licenses/

Takedown

If you consider content in White Rose Research Online to be in breach of UK law, please notify us by emailing eprints@whiterose.ac.uk including the URL of the record and the reason for the withdrawal request.

UNIVERSITY OF LEEDS University of Sheffield UNIVERSITY of York

Flame impingement to facilitate the stability of NH_3-CH_4 laminar diffusion flames: High-speed imaging and schlieren visualization

Yidu Tong[a], Chenyang Fan[a*], Zheng Fu[a,b], Ye Liu[c], Huiyong Du[a], Bin Xu[a], Guorong Lin[a], Shuo Jin[a], Shuainan Yang[a], Mingliang Wei[b]**

[a] Henan Provincial International Joint Laboratory of Energy Conservation and Pollutant Control of Energy Power Equipment, College of Vehicle and Traffic Engineering, Henan University of Science and Technology, Luoyang 471003, China

[b] State Key Laboratory of Intelligent Agricultural Power Equipment, Luoyang 471003, China

[c] Institute for Transport Studies, University of Leeds, Leeds LS2 9JT, UK

Corresponding author: Chenyang Fan

E-mail address: fanchenyang@haust.edu.cn; fanchenyang@tju.edu.cn

Postal address: College of Vehicle and Traffic Engineering, Henan University of Science and Technology, Luoyang 471003, China

***** Corresponding author: Ye Liu***

E-mail address: Y.Liu8@leeds.ac.uk

Postal address: Institute for Transport Studies, University of Leeds, Leeds LS2 9JT, UK

Abstract

As a hydrogen-rich and carbon-free fuel with high energy density, ammonia is regarded as a promising substitute for fossil fuels. In this study, flame characteristic and flow field were investigated to explore the maximum substitution ratio of ammonia (critical substitution ratio, i.e.) in NH_3-CH_4 by high-speed direct imaging and schlieren method. To follow up the realistic scenario of flames in enclosed combustion systems, the stability of impinging flame was also investigated under the effect of water-cooled cooper wall. The results showed that the critical ammonia substitution ratio for free laminar flames was less than 63% for the tested cases. Meanwhile, the free flames exhibited periodic expansion and separation, with significant fluctuations in lift-off height and flame stretch rate, accompanying with the periodic motion of the shear layer between the flame and air. After the introduction of the impinging wall, the critical ammonia substitution ratio of the flame increased from 63% to over 80% (up to 94%) in dependent upon the height of impinging wall. At low ammonia substitution ratio (40%), reducing the impinging height enhanced the stability of the flow field by suppressing the development of shear layers and vortex around the flame. When the ammonia substitution ratio gradually increased to 63% and the critical substitution ratio, the flame anchored on the wall at different impingement heights, and no obvious vortex development was observed in the flow field. Higher ammonia substitution ratios can weaken the influence of impingement height on the flame flow field.

Keywords: Ammonia combustion; Impinging flame; Flame stability; Schlieren technique; Vortex

Nomenclature

Re	Reynolds number
Le	Lewis number
D	Inner diameter of burner nozzle (mm)
H_b	Length from nozzle exit to root of lift-off flame (mm)
R_r	Radius of flame root (mm)
R_t	Radius of flame tip (mm)
κ	Flame stretch rate (s^{-1})
A_f	Projected area of flame yellow luminescent region (mm^2)
α	Ammonia substitution ratio
α_{cr}	Critical ammonia substitution ratio
Q_f	Fuel flow rate (SLPM)
H_I	Distance between nozzle and impinging wall (mm)
β	Ratio of the H_b to the D
H_v	Length between vortex position and nozzle exit (mm)
V_x	Axial motion velocity of vortex (m/s)
H_r	Distance between flame root and impinging wall (mm)

1. Introduction

With the rising demand for clean energy, ammonia (NH_3) has attracted attention as a sustainable fuel [1-3]. As an excellent hydrogen carrier, NH_3 is a carbon-free and high energy density fuel which can be stored and transported safely with advanced facilities [4, 5]. Thus, NH_3 is regarded as a non-hydrocarbon based fuel that may be applied in combustion systems such as gas turbines [6], internal combustion engines and industrial furnaces [7-9]. However, studies have shown that NH_3 has inferior combustion characteristics, including low laminar burning velocity and high minimum ignition energy requirement [10, 11]. These characteristics limit the practical application of NH_3. Co-combustion of NH_3-CH_4 mixed fuel with CH_4 accounting for 70% has a burning velocity 2.14 times higher than that of pure NH_3 flames, and thus is widely used in various combustion devices for practical applications [10, 12].

Flame stability constitutes a critical issue for industrial applications and remains a subject of extensive studies. Lin et al. [13] reported that in ammonia-methane laminar diffusion flames, increasing ammonia fraction from 30% to 50% reduced flame flickering frequency and shifted vortex formation downstream. Colson et al. [14] similarly observed this phenomenon, attributing it to reduced mixture reactivity with ammonia addition, which stabilized flames farther downstream where local velocities were lower. In the study of Zheng et al. [15] about instability for ammonia-methane non-premixed flames, they found that as the ammonia content increased to 40%, the flame would transition from turbulent to laminar lifted flame and be directly extinguished from laminar lifted flames. The study of Colson et al. [16] on the stability of non-premixed methane jet flames found that the flame can't be stabilized when the ammonia ratio exceeds 0.3. Thus, to better utilize ammonia, increasing the ammonia substitution ratio in ammonia-methane blended fuels and enhancing flame stability under high ammonia substitution ratios are imperative.

Numerous studies have indicated that the flame instability or extinction behavior is primarily influenced by three factors: chemical reactions [17], thermal instability [18], and flow instability [19]. Won et al. [20] studied the chemical kinetics of hydrocarbon fuel (n-alkanes and iso-octane) diffusion flames. They found that hydroxyl (OH) radicals are key reactive intermediates in the oxidation reactions of hydrocarbon fuels and the concentration of OH radicals affect the rate of chain reactions related to alkane pyrolysis. Insufficient supply of OH radicals leads to a decrease in decomposition rate, making combustion unsustainable. Furthermore, there is a positive feedback relationship between the generation and consumption rate of OH radicals and the heat release rate in the flame, thereby affecting flame extinction. Chu et al. [21] found that the addition of NH_3 lessened the production of OH radicals in the methane flame, thereby making the flame easier to extinguish. In the study of Chen et al. [17] on ammonia-methane counterflow diffusion flames, increasing the initial pressure and temperature could compensate the negative effect of ammonia addition on flame instability, thereby increasing the ammonia substitution ratio. They attributed this phenomenon to the fact that elevated initial pressure and temperature could accelerate chemical reaction efficiency and increase heat release. Increasing the initial pressure and temperature during combustion may be one of the methods to improve the ammonia substitution ratio.

For practical applications on combustion systems (engine chambers, *etc.*), impinging flames have received considerable attention [22]. In despite of the thorough investigation on the stability characteristics of NH_3-CH_4 jet flames, the NH_3-CH_4 impinging flames may have distinctly different structures and dynamics and requires further understanding on the stability characteristics. Several studies investigated the influence of impinging wall on the combustion characteristics of hydrocarbon or ammonia-blended flames. Study on methane impinging flames have shown that the wall distance significantly affects the flame structure and near wall chemical reaction rate, potentially leading to local extinction [23]. In terms of flow field structure, vortex structures generated at the junctions of the primary jet region, wall jet region, and stagnation flow region disrupt the continuity of the flame front, triggering oscillations and reducing stability [24]. When ammonia is blended into the fuel, these effects become more pronounced. Research indicates that the addition of ammonia decreases the peak flame temperature and makes non-premixed impinging flames more prone to local extinction in the wall jet region [25]. On the other hand, for premixed flames, wall impingement can enhance stability by reducing the flow velocity around the flame, thereby enabling a higher ammonia blending ratio [26].

The previous studies investigated the effects of adding ammonia and impinging wall on flame stability, especially in chemical reactions. However, the maximum ammonia substitution ratio in ammonia-methane flames and the dominant factors related to the flame stability near the critical ammonia substitution ratio need further investigation under the coupling effect of ammonia and impinging wall. In this study, a combination of high-speed direct imaging and schlieren method was utilized to analyze the flame structure and dynamic characteristics. The promoting effect of the impinging wall on the critical ammonia substitution ratio was obtained by comparing the differences in flame structure and stability between NH_3-CH_4 free flames and impinging flames. The critical ammonia substitution ratios under different impinging heights were obtained. Additionally, the evolution of the flame flow field was investigated to shed light on its effect on flame stability. The present work may enrich the understanding of NH_3-CH_4 impinging flames and facilitate the application of ammonia fuel on combustion systems.

2. Experimental description

The set-up of experimental apparatus is shown in Fig.1, consisting of a McKenna flat-flame burner, mass flow meters and a water-cooled copper plate. Acrylic cover was enclosed on the laminar diffusion flame to mitigate environmental interference. The burner with a fuel nozzle inner diameter (*D*) of 8 mm, surrounded by a 60 mm diameter coaxial air annulus, contains an Archimedes spiral cooling circuit for water flow to minimize radial temperature gradient. CH_4 and NH_3 with purity of 99.99% were supplied to the burner at given mass flow rates. A water-cooled copper plate with a size of 150 mm × 100 mm and a thickness of 10 mm was positioned directly above the burner to study the flame impingement process. Six water channels were built in to fix the plate temperature to 313±2 K through circulating water connected to thermostatic water bath (THS-10, Tianheng, China).

The optical measurement system includes a high-speed camera and the Z-type schlieren imaging system. A high-speed camera (Memrecam GX-8, NAC) was used to capture the configuration and structure of flame. All flame images (1024 × 1024 pixels) were recorded at a frame rate of 50 fps. A Z-type schlieren imaging system (HGD-SD200) is mainly composed of a 300 W tungsten halogen lamp and two concave mirrors. The Halogen Tungsten lamp was employed due to its continuous spectrum in the visible range, providing stable and broad light output. Each mirror has an effective diameter of 200 mm and a focal length of 2000 mm. It was used to investigate the density gradient of flame flow field and obtain the flame stretch ratio. Schlieren imaging was performed using a direct visualization technique, with all image sequences acquired at identical frame rates (500 fps) and shutter speeds to ensure temporal consistency across experimental conditions.

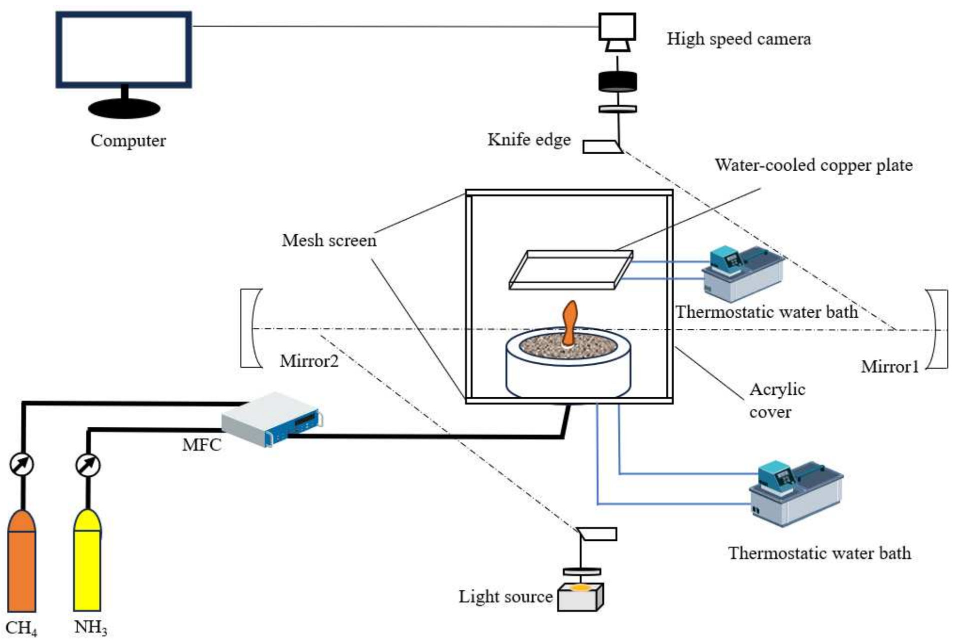

Fig.1 Experimental set-up.

Each flame image is converted into a binary image based on OTSU algorithm [27]. The algorithm distinguishes the flame boundary by assigning binary values (1 for flame and 0 for background). Then, the binarized images are further scrutinized to extract the flame dimensional parameters in terms of the height of lift-off (H_b), the radius of flame root (R_r), and the radius of flame tip (R_t), as depicted in Fig. 2(b). The H_b defined as the length from the nozzle exit to the root of lift-off flame. To characterize the flame stretch rate (κ) of impinging flames, the projected area of the flame yellow luminescent region (A_f) in the binarized images are measured. The κ is obtained according to the method of Chung et al. [28]:

$$\kappa = {}^{1}\!/_{A} \cdot {}^{dA}\!/_{d\tau} \tag{1}$$

where A represents the area of the flame surface, τ denotes the time scale, and dA/dτ is the rate of change of the flame area with respect to time. In terms of boundary processing, for the first and last frames of the flame images, the forward difference [29] and backward difference [30] methods were adopted for calculation, respectively. For the flame images in the middle, the central difference method was used [31].

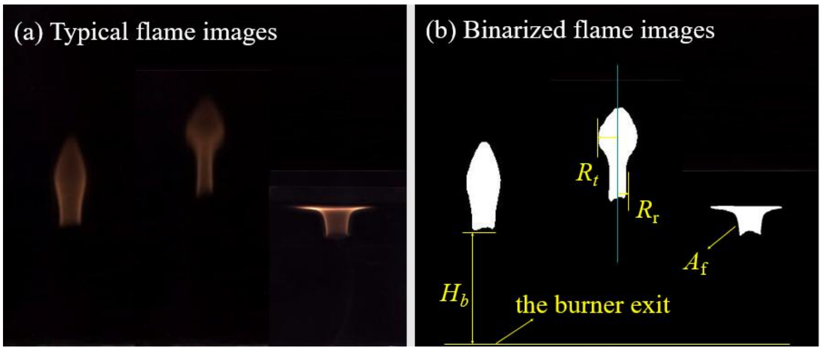

Fig. 2 (a) Typica images of free and impinging flame and (b) definitions of flame dimensional parameters.

In this study, the effects of different ammonia substitution ratios (α) in the fuel mixture and cold-flow Reynolds numbers (Re) on flame stability were investigated. These parameters are defined by Eq. (2) and Eq. (3), respectively. The flow rate of CH_4 and NH_3 were controlled by mass flow meters (AB-11, AiroBoost) with an accuracy of

1% of full scale. The ammonia substitution ratio exhibited a ±1% experimental uncertainty due to pressure fluctuation of fuel flow and systematic calibration deviations of the mass flow meters. Each test condition was conducted with more than three repeated experimental trials. The results derived from the flame images were averaged, with error bars representing the deviations from multiple repeated experiments.

$$\alpha = \frac{Q_{NH_3}}{Q_{NH_3} + Q_{CH_4}} \tag{2}$$

$$Re = \frac{\rho_{mix} V_{mix} D}{\mu_{mix}} \tag{3}$$

Where Q represents the volumetric flow rate of gases, and ρ_{mix}, V_{mix}, and μ_{mix} represent the density, velocity, and viscosity coefficient of the fuel mixture, respectively. Additionally, D is the inner diameter of the nozzle.

In this study, critical ammoniasubstitution ratio (α_{cr}) in NH_3-CH_4 diffusion flames under different experimental conditions were investigated experimentally. For free flame without impinging wall, three fuel flow rates (0.7 slpm, 0.8 slpm, 0.9 slpm) were set as shown in Tab. 1, and α was continuously increased to obtain the threshold of ammonia proportion of NH_3-CH_4 free flame. In the experiment, the threshold of ammonia proportion beyond which the flame tuned to an instable nature was recorded as the α_{cr}. The instable nature refers to the phenomenon that the flame boundary continuously fluctuates until eventual blow-out. Subsequently, a water-cooled copper plate was introduced to establish an impinging flame. The flame behavior patterns were found to be consistent across all three flow rates in free flames. Therefore, the impinging flame experiments were conducted with the representative flow rate of 0.8 slpm. Various impinging height (H_I), defined as the vertical distance between the exit of burner nozzle and the water-cooled copper plate, corresponding to 3, 6, 9 and 12 times the nozzle inner diameter were adopted for the impinging flame experiments. To eliminate the interference of wall temperature on the experiment, the plate temperature was retained at 313 ± 2 K through a thermostatic water bath.

Tab.1 Test conditions.

Case	Fuel flow (SLPM) Q_f	H_I (mm)	Critical ammonia substitution ratio (α_{cr})	Cold flow Reynolds number under α_{cr} (Re)
F1	0.7	/	63%	118.09
F2	0.8	/	63%	134.96
F3	0.9	/	63%	151.83
I1	0.8	24	84%	137.43
I2	0.8	48	87%	137.79
I3	0.8	72	94%	138.62
I4	0.8	96	91%	138.14

3. Results and discussion

3.1 Threshold of ammonia substitution ratio for flame extinction

3.1.1 Free diffusion flame

In our previous work [13], flame instability in NH_3-CH_4 laminar free diffusion flames was investigated at up to 50% substituted ratio of NH_3. It was found that upon ammonia addition, flames exhibit recurrent periodic oscillations similar to pure methane flames. In this study, the α is further elevated to explore the mechanism for why the flame instability occurs. After further increasing the α ($\geq$60%), the flame possesses a more pronounced lift-off height and appears a blow-out as α_{cr} is achieved. As the ammonia substitution ratio reached the threshold, high-speed camera was triggered simultaneously with flame ignition to capture the blow-out process. The flame exhibited periodic contraction oscillations, followed by a marked decrease in lift-off height. Fig. 3(a) shows the flame periodic oscillation process under various Q_f at α_{cr}. The periodic oscillation of flame arises from the following mechanisms: differences in velocity and density between the fuel and air form the shear layer, within which oxidation reactions of the fuel release heat that induces thermal expansion [32]. Thermal expansion exacerbates the density difference, and together with gravity, generates buoyancy. Driven by thermal expansion and buoyancy, the shear layer increases in diameter and forms vortex. The pushing or pulling effects of vortex on the flame surface cause local extinction and flame separation [33]. The shear layer repeats the developmental process, ultimately resulting in the periodic oscillation of the flame. Subsequently, the flame root undergoes a progressive elevation, contraction and expansion, ultimately leading to necking phenomena that detach the protruding region of the flame as time evolves, and eventually flame extinguishes as shown in Fig. 3(b). Necking originates from vortex generated by the shear layer between the jet and the ambient air, producing critical flame stretch rates that peak within the constricted region [34]. Enhanced flame stretch induced by flame surface curvature can trigger local extinction and necking [28]. Subsequently, the flame extinguished in both upward and downward directions.

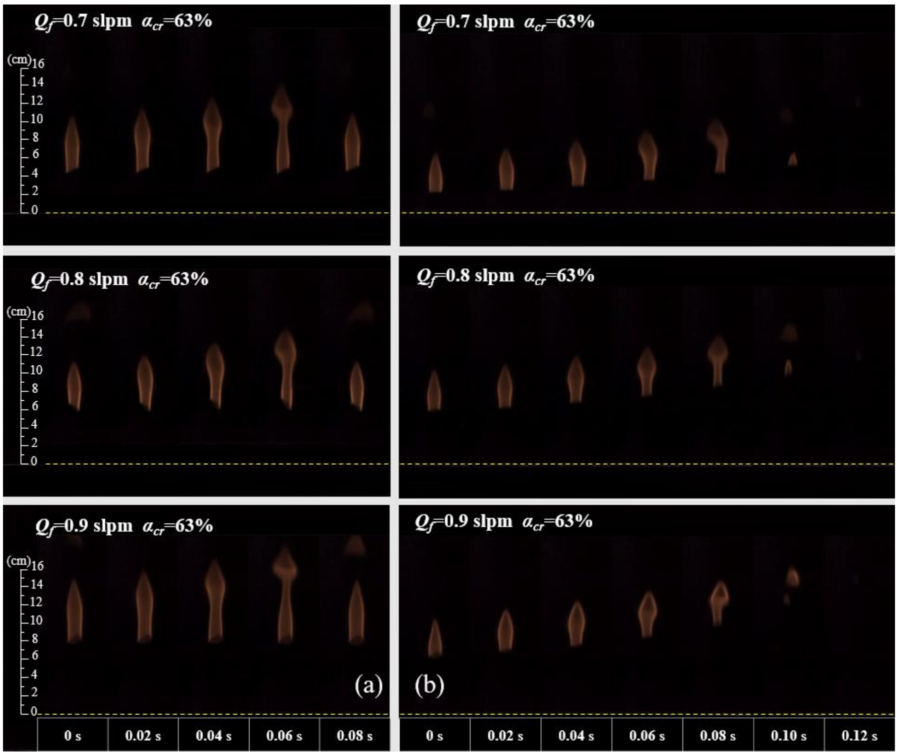

Fig. 3 The extinction process of NH_3-CH_4 free diffusion flame: (a) first sequence after ignition; (b) last sequence preceding flame extinction. (The yellow dashed lines represent the burner nozzle exit.)

To clearly observe flame evolution from ignition to extinction, the minimum and maximum of H_b within each oscillation cycle were obtained, as well as the maximum values of R_t and minimum values of R_r. As shown in Fig. 4(a) and (b), both H_{b_min} and H_{b_max} undergoes a reduction-then-increase trend as the time evolves under the various Q_f. Furthermore, when the Q_f increases from 0.7 to 0.8 slpm, H_{b_min} and H_{b_max} correspondingly raise. However, upon further increase to 0.9 slpm, a higher magnitude of reduction is observed and the minimum values of H_{b_min} and H_{b_max} are even lower than that for 0.8 slpm. According to the study of Lin et al. [13], when shear layer vortices reach a critical threshold, they trigger global flame lift-off, and ammonia addition enhances this phenomenon. Concerning lift-off conditions, Takahashi et.al [35] proposed that a lift-off occurs when the local flow velocity at the flame base exceeds flame laminar burning velocity. Due to the relatively small laminar burning velocity of ammonia, as α increases, the flame laminar burning velocity will significantly decrease [36, 37], facilitating the lift-off flame phenomenon. Similar phenomena were also observed in the study of Zheng et al. [15] on the unstable characteristics of NH_3-CH_4 non-premixed jet flames. They found that for the fixed ammonia substitution ratio, increasing the fuel injection speed would cause the flame to transition from an attached flame to a lift-off flame and further increasing the fuel injection speed would result in an increase in H_b. Similarly, Fig. 4(c) and (d) reveal that R_{t_max} and R_{r_min} exhibit an overall trend of initially irregular fluctuations across various Q_f, followed by a steep decline during the final 3~6 oscillation cycles preceding extinction. Quantitatively, R_{t_max} and R_{r_min} increase correspondingly with higher Q_f across the tested range. The aforementioned dynamics phenomenon is a comparison of three cases under free diffusion flame. Given their consistent behavioral pattern as a whole, a representative flow rate of 0.8 slpm was selected as the Q_f for subsequent impinging flame experiment.

The non-monotonic structure variation and eventual blow-out of the NH_3-CH_4 free flame at α_{cr} indicate that a high ammonia substitution ratio leads to a significant decrease in laminar burning velocity, thereby intensifying the global extinction phenomenon induced by shear layer vortex [38]. For the flame impingement condition, the axial velocity of the unburned gas flow in the stagnation zone will be significantly reduced due to impingement on the wall, while the flow in the near wall jet region will be significantly affected by the boundary layer [26]. Therefore, the impingement process can establish a flow field with a lower velocity than that in the free flame, which is ultimately conducive to establishing a more stable flame shape and a complete flame front. In this case, further investigation on the effect of the impinging wall is conducted and explore whether and how the impinging wall can further extend the threshold of ammonia substitution ratio.

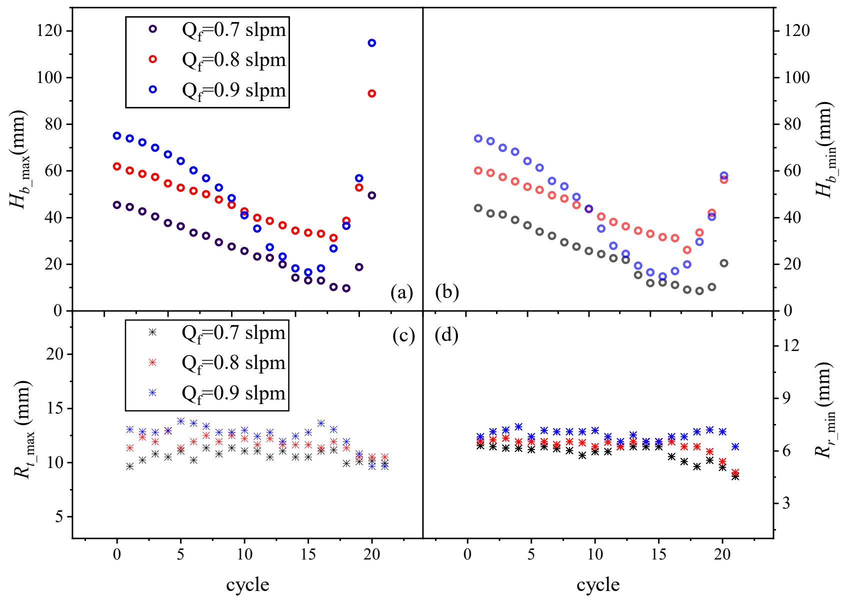

Fig. 4 Variation of flame size parameters over cycle: (a) the maximum height of lift-off (H_{b_max}) with various fuel flow rate (Q_f); (b) the minimum height of lift-off (H_{b_min}) with various Q_f; (c) the maximum radius of the flame tip (R_{t_max}) with various Q_f; (d) the minimum radius of flame root (R_{r_min}) with various Q_f.

3.1.2 Impinging flame

To evaluate the effect of the impinging wall on laminar diffusion flames, experiments on NH_3-CH_4 diffusion impinging flames with different α are conducted at a constant Q_f of 0.8 slpm by varying the H_I. At the same α, the appearances of NH_3-CH_4 impinging flames differ from that of free flames, as shown in Fig. 5. Under this condition, the necking and separation characteristic of free flames are not appeared by the impinging flame that instead exhibit a stable lift-off flame attached to the impinging wall. A further analysis of Fig. 5 reveals that H_b increases with the increase in H_I. A dimensionless parameter β, defined as the ratio of the lift-off height (H_b) to the nozzle inner diameter (D) is used to reveal the effect of H_I.

$$\beta = H_b / D \quad (2)$$

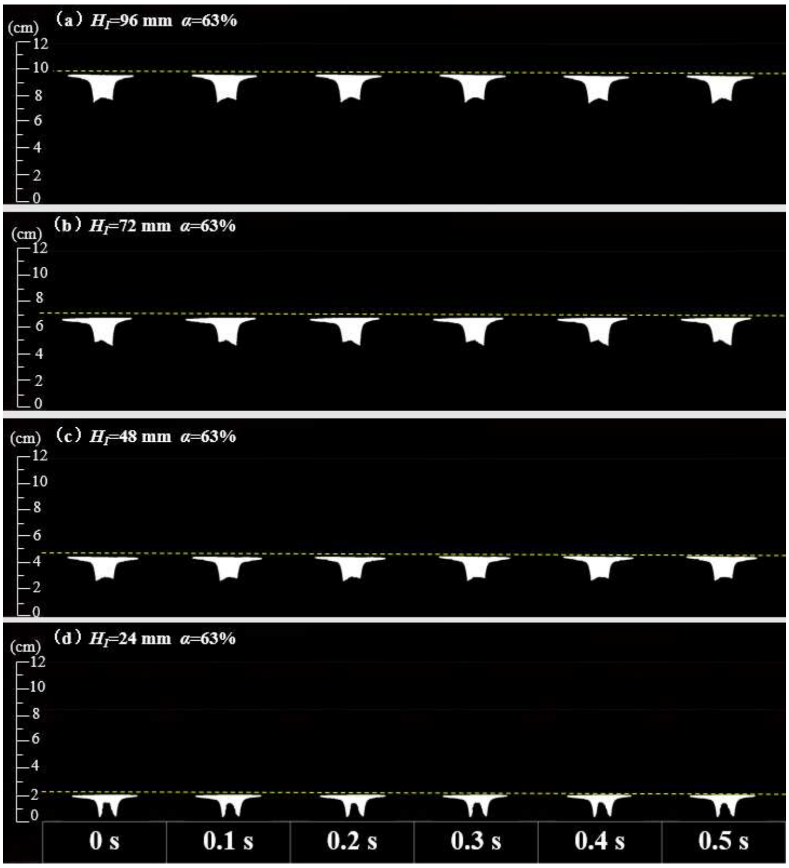

Fig. 5 Sequence diagrams of binarized images of impinging flame at different impinging heights (H_I) under the fuel flow rate (Q_f) of 0.8 slpm and the ammonia substitution ratio (α) of 63%, with the yellow dashed line denoting the position of the water-cooled copper plate.

For comparison with free flames at α of 63%, the cycle experienced by the free flame from ignition to extinction is defined as the period of interest. Given that the impinging flame does not extinguish, flame images captured at equal time intervals are used to quantify the corresponding parameter. The results in Figs. 6-8 are the mean values obtained for each cycle. Fig.6 shows the variation of β for free flames during the extinction process and that for imping flame under different H_I. It is observed that for the impinging flame β increases with the rise in impinging height. Besides, it is noted that adjusting H_I improves the flame stability. When H_I decreases from 48 mm to 24 mm, β drops to around 0.4, indicating that reducing H_I facilitates the transition of the flame from lifted to attached state. Furthermore, the β of the impinging flame exhibits marginal fluctuations over the whole period, which indicates a stable combustion. In contrast, β for the free flame shows significant fluctuations. This phenomenon is related to the above-mentioned necking and separation occurring in the free flame. Vortex beneath the bulge of the free flame tip pushes the flame surface outward, while vortex above the bulge pulls the surface inward, thereby enhancing fuel and air mixing at specific moments [39]. As a result, the local burning velocity and stretch rate increase, leading to fluctuations at the flame boundary.

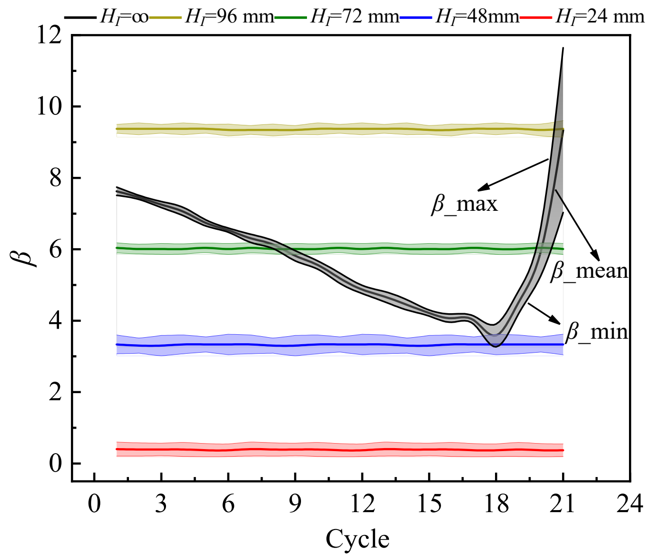

Fig. 6 Variation of the ratio of the lift-off height to the nozzle inner diameter (β) for different impinging heights (H_I) at the fuel flow rate (Q_f) of 0.8 slpm and the ammonia substitution ratio (α) of 63% with cycle (where the impinging height of ∞ corresponds to the free flames).

A_f for flames under different H_I are derived from the binarized images, as shown in Fig. 7. A_f for the free flames exhibit a significant fluctuation amplitude over cycle, particularly during the latest cycles of the flame extinction process. This behavior corresponds to the aforementioned changes in β. After the introduction of the impinging wall, the variation amplitude of A_f decreases, further verifying the improvement in flame stability. In addition, A_f shows a significant reduction with the introduction of impinging wall, and gradually increases with the increasing H_I. However, when the H_I increases from 72 mm to 96 mm, A_f shows no significant increase and sustains a comparable level. Similar phenomenon was also found by Zhen et al. [40]. In the presence of an impinging wall, the conical shape of the flame front is truncated by the wall, causing radial stretch of flame and restricting the axial development, finally resulting in the flame taking on 'V' and 'M' shapes. For impinging flames, Li et al. [23] found that as the impinging height increases, the flame shape changes from a horn-like form to a complete shape. They explained that the space for flame development expanded with an increase in impinging height, permitting more ambient air entrained into the combustion zone, resulting in more thorough combustion and an enlarged flame area.

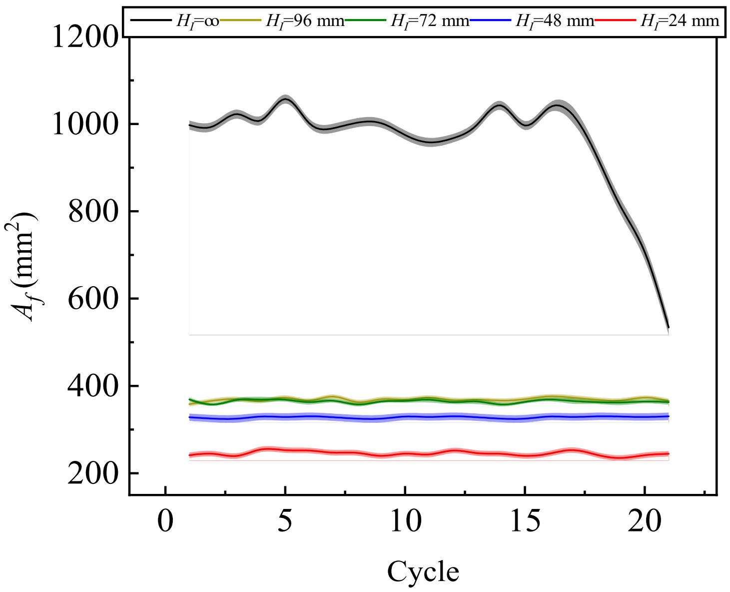

Fig. 7 Variation of projected area of the flame yellow luminescent region (A_f) for different impinging heights (H_I) at the fuel flow rate (Q_f) of 0.8 slpm and the ammonia substitution ratio (α) of 63% with cycle.

Flame stretch rate (κ) is also employed to quantify the improvement of flame stability by wall impingement. As shown in Fig. 8, κ for the impinging flames are nearly zero, indicating that the flame area varies slightly and tends to a stability. For $H_I \geq 48$ mm, κ shows moderate fluctuate and exhibit no significant affinity with the variation in H_I. Surprisingly, for H_I of 24 mm, κ shows marginal fluctuation in the early cycle, but present a large amplitude fluctuation in the later cycle. In contrast, the free flames exhibit higher level and fluctuation amplitude (-4~5) in κ, suggesting severe changes in A_f. According to Jung et al. [41], larger flame stretch rate reduces the flame heat release rate, inhibiting heat release in the reaction zone, and ultimately leads to flame extinction. In the last 7 cycles before the extinction of the free flame, κ remained negative, suggesting a continuous decrease in A_f until extinction. This phenomenon may be related to the rates of mass diffusion and thermal diffusion in the flame, i.e. the Lewis number (*Le*) of the fuel. *Le* for NH_3 is significantly higher than that for CH_4 [42-44]. In the study by Zhang et al. [45], it was found that in the tip region of ammonia-methane flames, the preferential diffusion effect induced by the high Lewis number leads to insufficient local fuel mass diffusion and contraction of the flame area, which further causes flame contraction and eventually results in extinction.

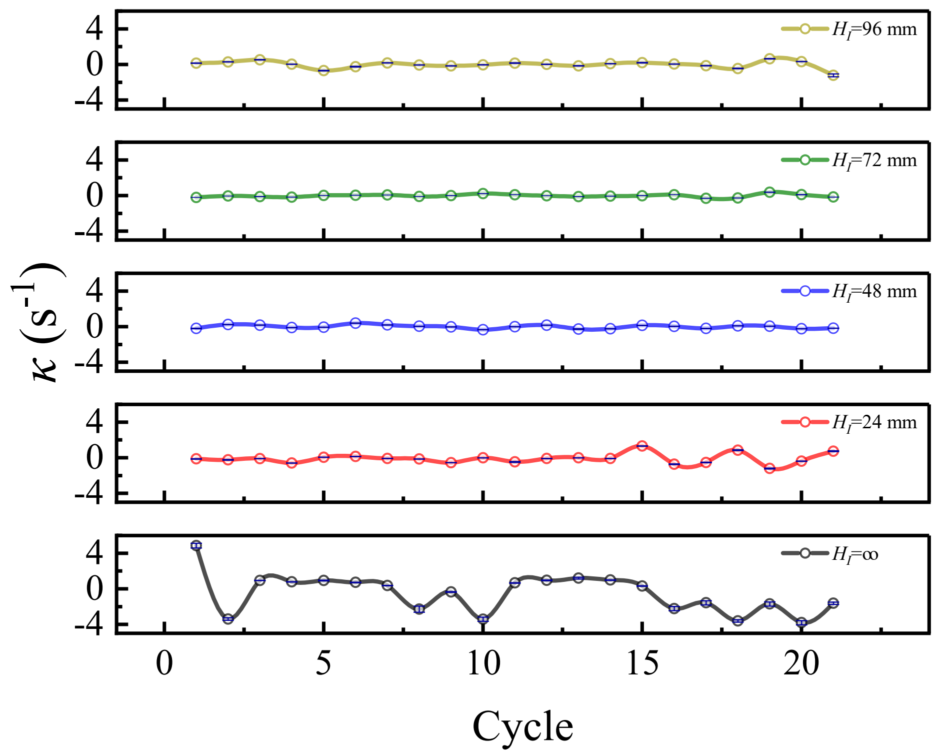

Fig. 8 Variation of flame stretch rates (κ) of flames for different impinging heights (H_I) at the fuel flow rate (Q_f) of 0.8 slpm and the ammonia substitution ratio (α) of 63% with cycle.

The α is further expanded to explore the maximum level of ammonia application in NH_3-CH_4 fuels. Compared with the free flame, α_{cr} for the impinging flame increases significantly, rising from 63% to over 80%, as shown in Fig. S1 of the supplementary material. This phenomenon indicates that the impinging wall enhances the stability of flames and α_{cr} is greatly improved. In laminar diffusion flames, the flame burning velocity and the flow velocity of the unburned gas are the key factors determining flame stability. The impinging wall may form a lower-velocity flow field matching the reduced laminar flame velocity for higher ammonia content, and facilitate the flame stability [26]. H_I is a crucial factor influencing the combustion characteristics of impinging flames [46]. As H_I increases from 24 to 72 mm, α_{cr} shows a monotonical increase and achieves the peak value of 94% at H_I of 72 mm. The impinging wall creates a stagnation flow field with a low velocity zone [24], reducing local stretch rate, as shown in Fig. 8. A lower κ can lead to a more stable flame anchoring, permitting a higher proportion of NH_3 to be substituted in the fuel mixture before reaching the critical condition. When H_I is further increased to 96 mm, the α_{cr} decreases to 91%. As H_I continues to increase, the flow becomes more complex with large fluctuations in the fuel-air mixture ratio and flow velocity. The non-homogeneous fuel mixture distribution and rapid changes in flow conditions make it difficult for NH_3 to burn efficiently. As a result, the flame stability deteriorates and α_{cr} decreases. At each H_I, the process from flame ignition to extinction under α_{cr} is recorded and digitalized with a time scale of 0.1 ms to derive the variations of β, A_f and κ over time.

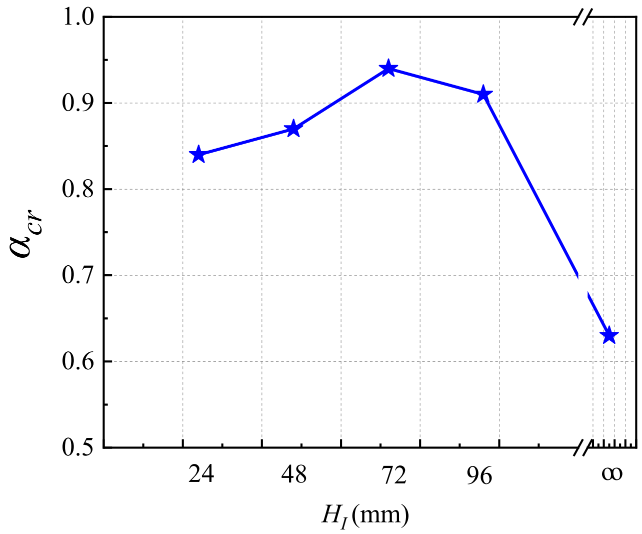

Fig. 9 Critical ammonia substitution ratio (α_{cr}) for different impinging heights (H_I) at the fuel flow rate (Q_f) of 0.8 slpm (where the impinging height of ∞ corresponds to the free flames).

As shown in Fig. 10, for the same H_I, β increases significantly with the increase in α, indicating that the flame base moves toward the upstream of flame. At the flame lift-off conditions [35], the local flow velocity equals to the flame burning velocity. As α further increases, the NH_3 addition further reduce the fuel burning velocity [36], and thus the flame root moves to downstream (with a lower flow velocity) to re-establish equilibrium. Meanwhile, the fluctuation amplitude of β increases as α further increases. At the initial α of 63% for the impinging flame, β shows nearly no temporal fluctuation. Conversely, at α_{cr}, β exhibits distinct fluctuations across different H_I, suggesting a deterioration in flame stability. The results of Colson et al. [47] indicated that the counterflow non-premixed ammonia-methane flames cannot be stabilized at higher ammonia constituted ratio (>70%) due to the flame weakness and strong buoyancy effect. At that condition, the flame resides in a regime proximate to the extinction limit, thereby exhibiting heightened susceptibility to perturbation, and β fluctuation increases. Additionally, further increasing α will also lead to an increase in *Le* of the fuel [43]. Wang et al. [48] found that on ammonia-methane laminar expanding flames, an increase in the *Le* leads to a more uneven distribution of flame surface curvature, exacerbating the geometric distortion of the flame surface. Owing to the high *Le* of NH_3, it is more sensitive to the interaction of vortex structure in the lifted state, resulting in the intensification of β oscillation under the lift-off condition.

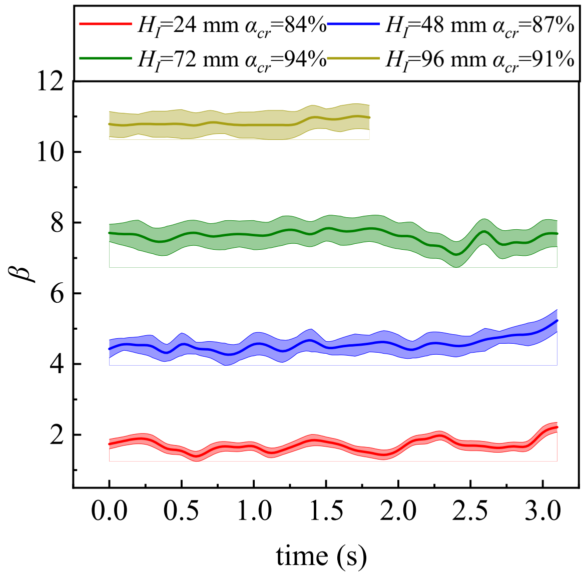

Fig. 10 Variation of the ratio of the lift-off height to the nozzle inner diameter (β) for different impinging heights (H_I) at the fuel flow rate (Q_f) of 0.8 slpm and the acritical ammonia substitution

ratio (α_{cr}) with time.

Under α_{cr}, A_f at different H_I all exhibit distinct fluctuations over time, as shown in Fig. 11. Meanwhile, as α increases from 63% to α_{cr}, A_f under different H_I decrease. The lower flame propagation speed, corresponding to a higher ammonia content , are prone to slow down the expansion rate of the combustion reaction zone and affect the mixing process of fuel and oxidizer [49], resulting in reduction in A_f. As H_I increased to 72 mm at which the largest α_{cr} is achieved, A_f is significantly larger than that at other H_I. The lower A_f at H_I of 24 mm and 48 mm may come from the strong cooling effect from the impinging wall on the flame front of the laminar flame [50]. When H_I further increases to 96 mm, A_f decreases significantly, and the combustion duration also reduces obviously. For this case, the cooling effect of the impinging wall on the combustion process may be diminished, while the entrainment of ambient air provides more oxidizer, exerting a significant cooling effect on flame combustion and leading to a reduction in A_f [51]. Similar to the free flame, A_f of the impinging flame gradually decreases until it extinguishes.

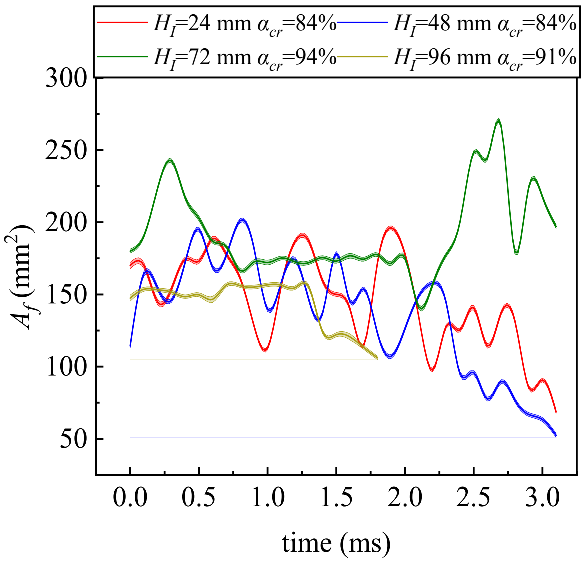

Fig. 11 Variation of projected area of the flame yellow luminescent region (A_f) for different

impinging heights (H_I) at the fuel flow rate (Q_f) of 0.8 slpm and the critical ammonia substitution ratio (α_{cr}) with time.

Fig. 12 shows the variation of κ with time at different H_I. At all impingement heights, κ possess periodical fluctuation over time. At H_I less than 48mm, the fluctuation amplitude of κ is relatively large (-3 to 4 s^{-1}). The flame is significantly affected by the wall, leading to the stretching and compression of the flame front at low H_I. As H_I increased from 48 mm to 72 mm, the fluctuation amplitude of κ decreases (-1 to 1.5 s^{-1}). At this time, the impinging flow field is stable, and the fuel and air may be mixed uniformly. When H_I increases to 96 mm, κ is relatively low in the early stage, but the fluctuation intensifies (-1.5 to 0.5 s^{-1}) in the later stage. At higher H_I, the fuel jet develops sufficiently, and the oxidizer is sufficient, but the turbulence intensity increases, which intensifies the local deformation of the flame front, resulting in larger fluctuations of κ in the later stage of combustion [52].

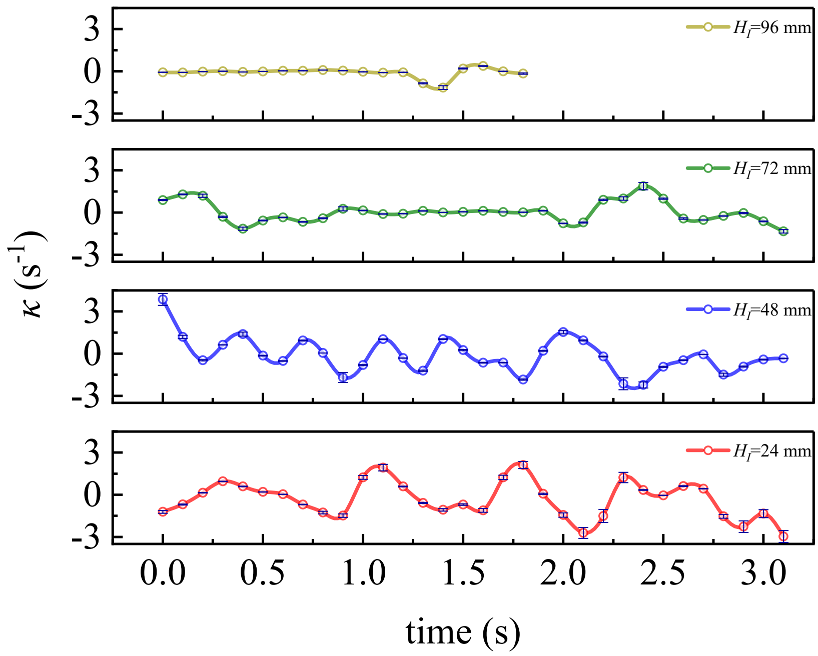

Fig. 12 Variation of flame stretch rate (κ) of flames for different impinging heights (H_I) at the fuel flow rate (Q_f) of 0.8 slpm and the critical ammonia substitution ratio (α_{cr}) with time.

3.2 Schlieren image analysis

Schlieren visualization is used to study the generation and distribution of vortex around flames and their interaction with flames [53, 54].

By changing H_I (24, 48, 72, 96 mm) and α (≥40%), the effect of impinging wall and ammonia substitution ratio on the stability of NH_3-CH_4 flame is obtained. Fig. 13(a) presents the schlieren image of typical impinging flame. There are three characteristic regions in the flow field: the primary jet region, the stagnation flow region and the wall jet region, which are consistent with the previous study of [55]. In the primary jet region, the impinging wall has no significant influence on the flow and the shear layer at the interface of flame and surrounding air presents a spindle shape, similar to the free NH_3-CH_4 laminar diffusion flame studied by Lin et al. [13]. In the stagnation flow region, the axial flow strongly decelerates and the radial flow accelerates, resulting in an increase in pressure and ultimately leading to the wall jet region. The wall jet region begins where the velocity is basically parallel to the impinging wall. In the wall jet region, the flame spreads along the wall surface.

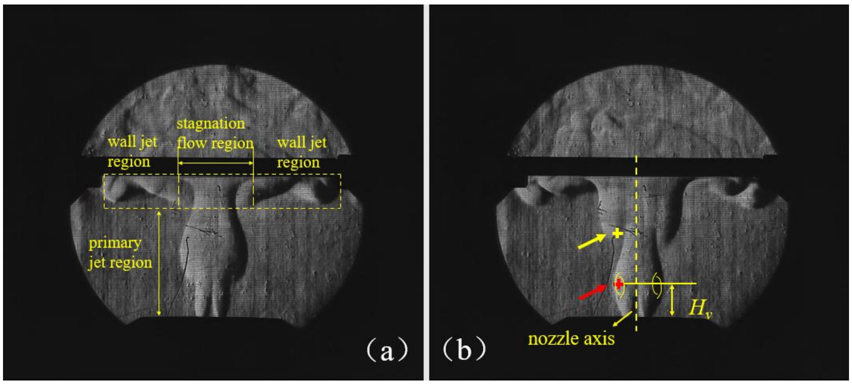

Fig. 13 (a) Schlieren diagram of the typical impinging flame; (b) schematic diagram of parameter definition.

A typical sequence of schlieren images depicting the development of flame vortex and their position in the flow field at H_I of 96mm and α of 40% is presented in Fig.14. In the primary jet region, the spindle-shaped shear layer at the flame and air interface undergoes periodic motion due to thermal expansion [56]. As shown in Fig. 14 , the flame vortex evolves sequentially: initial slight inward concavity (roll-up vortex) on the shear layer develops into an internal vortex with increasing shear layer diameter [57] Upon impingement, the axial development of the shear layer is constrained and gradually moving radially. At this time, the shear stresses near the wall generate an annular vortex in the near wall region [58, 59]. The vortex positions refer to the study by He et al. [59]. As the impingement distance increases, more vortex structures can be observed.

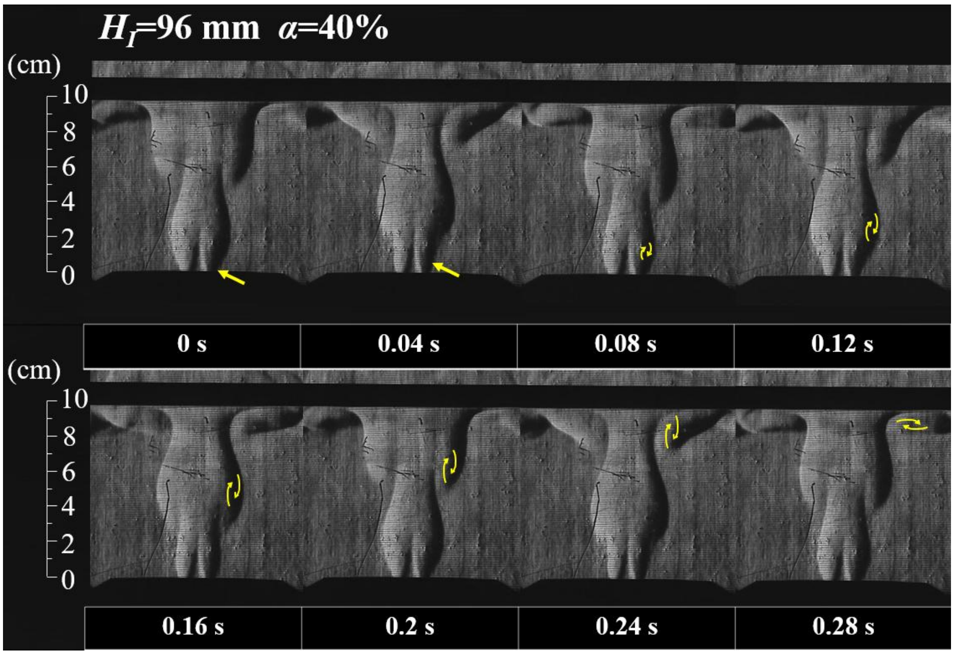

Fig. 14 Whole schlieren image sequence of flame vortex evolution at an impingement height (H_I) of 96 mm and an ammonia substitution ratio (α) of 40% (the yellow markers indicate the vortex positions)

Fig. 15 presents the complete sequence of schlieren images depicting the flames at α=40% for various H_I. At $H_I \geq 48$ mm, the spindle shaped shear layer undergoes periodic motion due to thermal expansion [13, 56]. Firstly, the shear layer expands gradually until the flame front impinges on the wall. Subsequently, the shear layer develops along the wall into a vortex - like shape. In contrast, with the lower H_I of 24 mm, the flame remains in a stable state in which the flame boundary exhibits negligible fluctuations, with no coherent vortical structures developing within the wall jet region. At lower impingement heights, the development of the fuel jet is constrained, leading to rapid dissipation of axial momentum [60]. The main jet region is compressed, which suppresses the development of flame vortex and alters the temperature distribution [59]. Consequently, a flow field distinct from that observed at other heights is formed. According to the study by Hsu et al. [57] on jet impinging on a flat plate, there are two axisymmetric vortices within each spindle-shaped shear layer, with the vortex center located at the maximum diameter of the shear layer, as shown by the red arrow in Fig. 13(b). After the flame impinges on the wall, the shear layer begins to stretch radially under the combined action of the wall and the original thermal expansion force, causing the alteration of the vortex center. The vertex center is the local extremum of the vorticity, therefore the new vortex center after flame impingement is obtained [24, 61], as depicted by the yellow arrow in Fig. 13(b). Therefore, to compare the influence of H_I on vortex development, the evolution of vortex center is studied. Red crosses track the development trajectory of the vortex, as shown in Fig. 15 (a-c). Initially, the spindle-shaped shear layer bends inward and forms roll-up vortex, depicted by the red arrows in the images. As time evolves, the elevation of vortex position with the development of the shear layer. After impinging on the wall, the flame front takes a V-shape and propagates radially along the wall. The difference in flame stability with the same α at different H_I indicates that reducing the H_I can mitigate the influence of vortex on flames by suppressing the development of flame shear layer, making it easier to achieve stable processes. In addition, the lower H_I allows more heat and active free radicals to be fed back to the unburned gas near the nozzle, which also helps stabilize the flame [62].

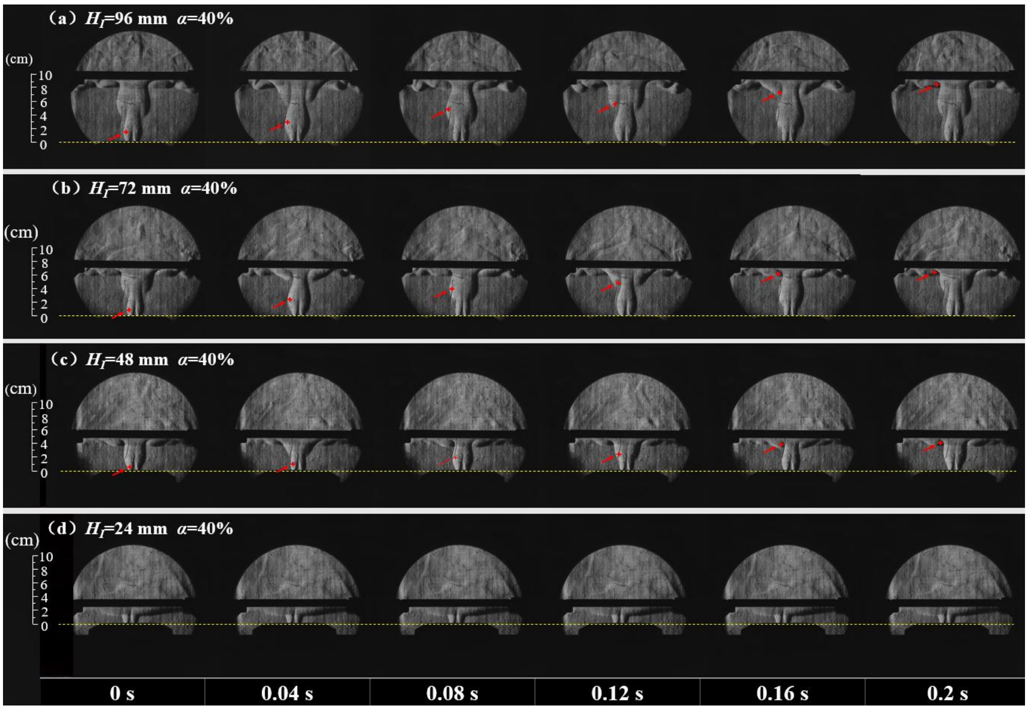

Fig. 15 Whole sequence of schlieren images for different impinging heights (H_I) at the fuel flow rate (Q_f) of 0.8 slpm and the ammonia substitution ratio (α) of 40%, with yellow dashed line represents the nozzle exit position.

The yellow horizontal line shown in Fig. 13 (b) represents the height of the vortex position (H_v), defined as the length between the vortex center and nozzle exit, which is used to calculate the axial motion velocity of vortex (V_x). Take the differential of H_v within the 0.04 s time interval to obtain V_x. The changes in H_v and V_x can be qualitatively used to describe the intensity of the vortex [63]. Fig. 16(a) shows the variation of H_v with time under different H_I. At all H_I, H_v gradually increases over time and eventually reaches a constant value. The reason is the low density hot gas enters the high density ambient air, causing the flame shear layer to expand continuously, and the vortex rises as the shear layer expands [64]. At 0.16 s, the vortex enters the wall jet region, the flame develops radially under the influence of the impinging wall, and H_v reaches a constant value. The V_x at different times is shown in Fig. 16(b). At each H_I, V_x shows the same variation law. At 0~0.08 s, the vortex is located in the primary jet region with little constraint by the wall and the vortex axial motion driven by thermal expansion force and jet momentum. The thermal expansion force causes a decrease in gas density near the flame front, forming an axial pressure gradient that accelerates the unburned gas and increases the flame burning velocity [65], resulting in an increase in V_x. At 0.08 s, the flame schlieren image shows that the flame tip collides with the impinging wall, causing the shear layer to be radially stretched and change of the vortex center. Subsequently, the wall stagnation effect gradually intensifies and exerts a reverse force on the flame through momentum exchange [66], leading to a significant decrease in V_x. At 0.12~0.16 s, the shear layer develops under the combined action of wall confinement and thermal expansion force, further increasing V_x. However, V_x in this case remains lower level than that before the impingement. After the vortex enters the wall jet region, it develops radially along the wall. As the radial distance increases, the vortex gradually dissipates and V_x decreases due to the influence of wall viscous resistance and shear stress [25]. Reduced H_I relocates vortex downstream, leading to reduction in V_x. The reduction of H_I shortens the primary jet region and may enhance the wall-induced stagnation effects, thereby weakening the axial acceleration driven by thermal expansion force. Consequently, shear layer and vortex development are suppressed, establishing a stable flow field as depicted in Fig. 15(d).

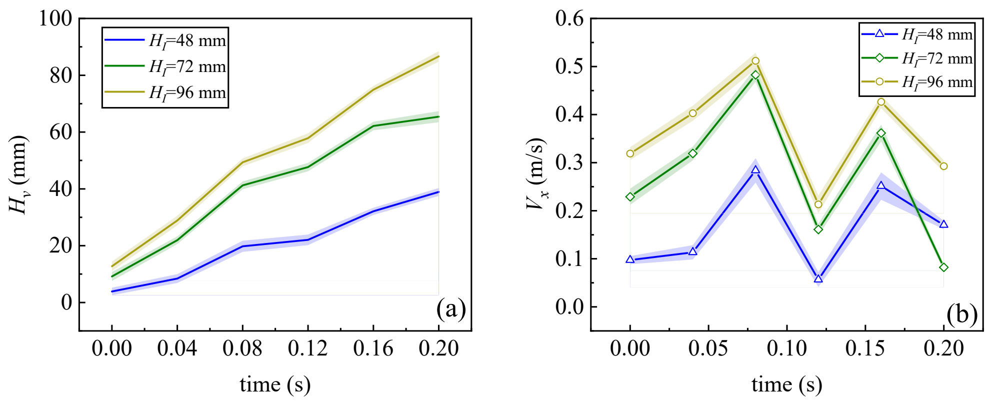

Fig. 16 Parameters of the vortex over time for different impinging heights (H_I) at the fuel flow rate (Q_f) of 0.8 slpm and the ammonia substitution ratio (*α*) of 40%: (a) the length between the vortex center and nozzle exit (H_v); (b) the axial motion velocity of vortex (V_x).

To further understand the influence of *α*, the flame schlieren images for higher *α* (63% and α_{cr}) at different H_I are shown in Fig. 17. At higher *α*, the flow field exhibits similar stable state at each H_I to that for H_I=24 mm of *α*=40%. Notably, for *α*=63%, as H_I elevates to higher value of ≥48 mm, the periodic development of shear layer and vortex vanishes and the flow field undergoes towards the stable state. He et al. [24] observed a similar phenomenon, in the near-wall region, the area of vortex significantly decreases with an increase in the NH_3 blending ratio. When further increases *α* from 63% to α_{cr}, the flow field stability remains unaltered under different H_I. However, the flame in the primary jet region moves downstream, and the motion of the flame flow field is mainly concentrated in the stagnation flow region and the wall jet region. That is, increasing *α* probably weaken the influence of H_I on the flame flow field, enabling the flame to stably attach to the wall for combustion.

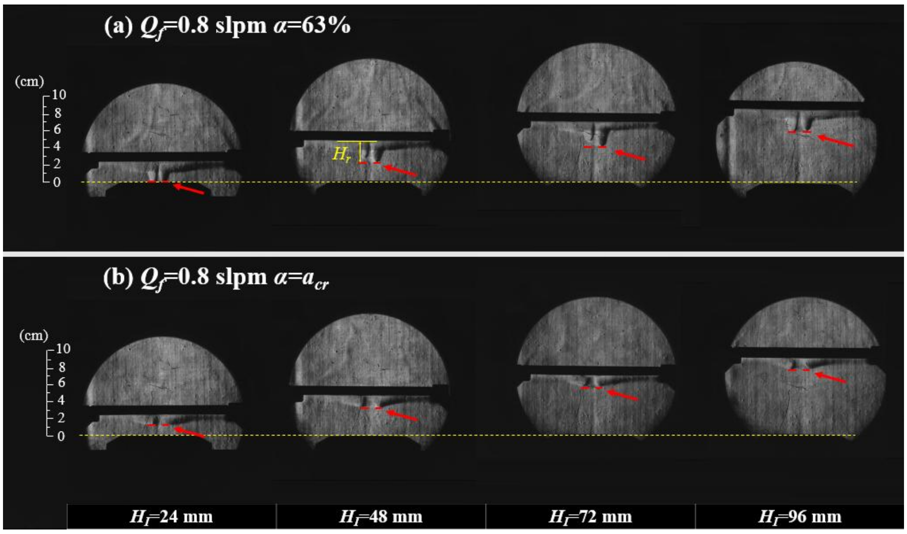

Fig. 17 Schlieren images for different impingement heights (H_I) and ammonia substitution ratios (α) at the fuel flow rate (Q_f) of 0.8 slpm, with yellow dashed line represents the nozzle exit position.

The distance between the flame root and the impinging wall, termed as H_r, is used to further depict the flow structure. The definition of H_r is demonstrated in Fig.17. As shown in Fig. 18, for α=63%, with increasing H_I, H_r gradually rises and reaches the peak at H_I=72 mm, then decreases slightly as H_I further increases to 96 mm. When further increasing to α_{cr}, H_r exhibits no consistent trend and scatters within a range of 12.5 mm to 13.5 mm, meaning that H_r may be insensitive to the variation in H_I. This phenomenon indicates that the increase of α may anchor the flame root in the near wall region, suppressing the effect of H_I on flow field. According to the study of Takahashi et al. [35], H_r is controlled by flame burning velocity and local fuel flow velocity. Higher ammonia content in flames reduces flame burning velocity, driving the flame root downstream and transitioning from attached flame to lifted flame configuration [36]. At $H_I \geq 48$ mm, the lifted flame shortens H_r, which may result in a flow field similar to that at H_I = 24 mm. Therefore, the impinging wall suppress vortex development and enhance flow field stability, thereby the lifted flame anchoring.

Conversely, at higher ammonia substitution (*α*=63%), the free flame undergoes necking as the shear layer develops, leading to flame instability and ultimately triggering blow-out probably.

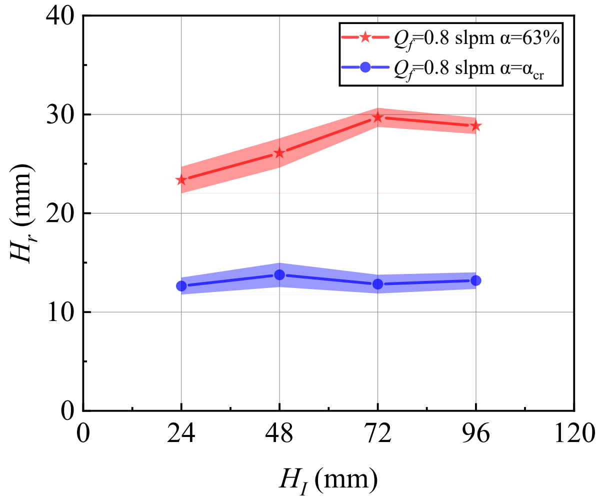

Fig. 18 The value of H_r under different impingement heights (H_I) at the fuel flow rate of 0.8 slpm.

In relevant studies, the extinction of NH_3-CH_4 flame has been extensively scrutinized and attributed to various factors such as fluid dynamics [19], chemical reactions [17] and thermal effects [18]. Under the critical substitution ratio of ammonia in hydrocarbon fuels, the development of flame vortex is suppressed and the flow instability within the flow field is weakened with the effect of the impinging wall. Thus, chemical reactions and thermal instability may be the main factors leading to flame extinction under the condition. This assertion is supported in the study of [59] on characteristics of methane non-premixed impinging flame. The high-temperature region was concentrated in the stagnation region, and the temperature gradually decreased as the wall-attached flame propagated. They attributed this phenomenon to the decrease in flame temperature caused by heat and momentum dissipation during the propagation of the wall-attached flame in the near wall region, which leads to weakened flame stability and extinction behavior. According to the study of Chu et al. [21], a decrease in flame temperature due to the addition of ammonia to methane non-premixed flames reduces the reaction rate and decreases the production of OH radicals, thereby resulting in a lower extinction limit of the flame. With the introduction of impinging wall, the flame flow field becomes jointly controlled by both impinging height and ammonia substitution ratio. The impinging wall likely enhances the critical ammonia substitution ratio primarily by altering vortex distribution and evolution within the flow field. Under the present experimental conditions, when ammonia substitution ratio reaches a certain level, it may weaken the effects of impinging height, causing flow fields to converge toward identical characteristics.

4. Conclusion

The effect of impinging wall on the stability of ammonia-methane laminar diffusion flame was investigated by the high-speed camera system and schlieren method in this work. The main findings are summarized as follows:

In the absence of the impinging wall, the free flame exhibits periodic expansion and separation at the critical ammonia substitution ratio, displaying pronounced fluctuations dominated by flow instability. With introduction of the impinging wall, the critical ammonia substitution ratio of the flame increases from 63% to over 80%. At a low ammonia substitution ratio (40%), reducing the impinging height promote the stability of flow field by suppressing the development of shear layer and vortex around the flames. When the ammonia substitution ratio is gradually increased to 63% and the critical substitution ratio, the flames are anchored on the wall at different impinging heights, with no significant vortex development in the flow field. Therefore, a higher ammonia substitution ratio can weaken the influence of impinging height on the flame flow field, and chemical and thermal instability may be the main factors leading to flame extinction under this condition. In addition to flow instability caused by flow field fluctuations, chemical kinetics and thermal instability in the flame are also key factors affecting flame stability. Therefore, the chemical kinetics and temperature effects of ammonia-methane flames under impinging wall conditions will be further investigated in our subsequent studies.

CRediT authorship contribution statement

Yidu Tong: Conceptualization, Investigation, Data curation, Visualization, Writing-original draft. **Chenyang Fan**: Investigation, Methodology, Funding acquisition, Supervision, Project administration, Writing-review and editing. **Zheng Fu**: Investigation, Resources, Validation. **Ye Liu**: Investigation, Validation. **Huiyong Du**: Methodology, Resources. **Bin Xu**: Methodology, Resources. **Guorong Lin:** Conceptualization, Visualization. **Shuo Jin**: Investigation, Data curation, Validation. **Shuainan Yang**: Investigation, Data curation, Validation. **Mingliang Wei**: Resources, Data Curation.

Acknowledgments

This research is sponsored by National Natural Science Foundation of China (No. 52006054), and International scientific and technological cooperation project in Henan Province (No. 232102521019).

References

[1] Kobayashi H, Hayakawa A, Somarathne KKA, Okafor EC. Science and technology of ammonia combustion. Proc Combust Inst 2019;37(1):109-33. https://doi.org/10.1016/j.proci.2018.09.029

[2] Ikäheimo J, Kiviluoma J, Weiss R, Holttinen H. Power-to-ammonia in future North European 100% renewable power and heat system. Int J Hydrog Energy 2018;43(36):17295-308. https://doi.org/10.1016/j.ijhydene.2018.06.121

[3] Smith C, Hill AK, Torrente-Murciano L. Current and future role of Haber–Bosch ammonia in a carbon-free energy landscape. Energy Environ Sci 2020;13(2):331-44. https://doi.org/10.1039/c9ee02873k

[4] Dolan RH, Anderson JE, Wallington TJ. Outlook for ammonia as a sustainable transportation fuel. Energy Fuels 2021;5(19):4830-41. https://doi.org/10.1039/D1SE00979F

[5] Valera-Medina A, Xiao H, Owen-Jones M, David WIF, Bowen PJ. Ammonia for power. Prog Energy Combust Sci 2018;69:63-102. https://doi.org/10.1016/j.pecs.2018.07.001

[6] Kurata O, Iki N, Matsunuma T, Inoue T, Tsujimura T, Furutani H, et al. Performances and emission characteristics of NH3–air and NH3CH4–air combustion gas-turbine power generations. Proc Combust Inst 2017;36(3):3351-9. https://doi.org/10.1016/j.proci.2016.07.088

[7] Frigo S, Gentili R. Analysis of the behaviour of a 4-stroke Si engine fuelled with ammonia and hydrogen. Int J Hydrog Energy 2013;38(3):1607-15. https://doi.org/10.1016/j.ijhydene.2012.10.114

[8] Vinod KN, Gore M, Liu H, Fang T. Experimental characterization of ammonia, methane, and gasoline fuel mixtures in small scale spark ignited engines. Appl Energy Combust Sci 2023;16:100205. https://doi.org/10.1016/j.jaecs.2023.100205

[9] Wang B, Wang H, Hu D, Yang C, Duan B, Wang Y. Study on the performance of premixed natural gas/ammonia engine with diesel ignition. Energy 2023;271:127056. https://doi.org/10.1016/j.energy.2023.127056

[10] Hayakawa A, Goto T, Mimoto R, Arakawa Y, Kudo T, Kobayashi H. Laminar burning velocity and Markstein length of ammonia/air premixed flames at various pressures. Fuel 2015;159:98-106. https://doi.org/10.1016/j.ijhydene.2015.04.024

[11] Zamfirescu C, Dincer I. Ammonia as a green fuel and hydrogen source for vehicular applications. Fuel Process Technol 2009;90(5):729-37. https://doi.org/10.1016/j.fuproc.2009.02.004

[12] Okafor EC, Naito Y, Colson S, Ichikawa A, Kudo T, Hayakawa A, et al. Experimental and numerical study of the laminar burning velocity of CH4–NH3–air premixed flames. Combust Flame 2018;187:185-98. https://doi.org/10.1016/j.combustflame.2017.09.002

[13] Lin G, Fan C, Fu Z, Li H, Liu Y, Du H, et al. Insight into the instability of ammonia-methane laminar diffusion flame. J Energy Inst 2025;119. https://doi.org/10.1016/j.joei.2024.101961

[14] Colson S, Kuhni M, Hayakawa A, Kobayashi H, Galizzi C, Escudié D. Stabilization mechanisms of an ammonia/methane non-premixed jet flame up to liftoff. Combust Flame 2021;234. https://doi.org/10.1016/j.combustflame.2021.111657

[15] Zheng J, Tang F, Chung SH, Hu L. Characteristics of liftoff, blowout and instability in nonpremixed jet flames with NH3/CH4 mixture fuels. Proc Combust Inst 2024;40(1-4). https://doi.org/10.1016/j.proci.2024.105591

[16] Colson S, Kuhni M, Galizzi C, Escudie D, Kobayashi H. Study of the combined effect of ammonia addition and air coflow velocity on a non-premixed methane jet flame stabilization. Combust

Sci Technol 2022;194(9):1747-67. https://doi.org/10.1080/00102202.2020.1830276
[17] Chen Y, Wang J, Zhang J, Li Y. Numerical Study on Chemical Kinetic Characteristics of Counterflow Diffusion Flame Extinction of Methane/Ammonia/Air Flame under High Pressure or Air Preheating Temperature. Molecules 2024;29(15):3632. https://doi.org/10.3390/molecules29153632
[18] Wang Y, Trouve A. Direct numerical simulation of nonpremixed flame–wall interactions. Combust Flame 2006;144(3):461-75. https://doi.org/10.1016/j.combustflame.2005.08.009
[19] Bradley D, Shehata M, Lawes M, Ahmed P. Flame extinctions: Critical stretch rates and sizes. Combust Flame 2020;212:459-68. https://doi.org/10.1016/j.combustflame.2019.11.013
[20] Won SH, Dooley S, Dryer FL, Ju YJC, Flame. A radical index for the determination of the chemical kinetic contribution to diffusion flame extinction of large hydrocarbon fuels. Combust Flame 2012;159(2):541-51. https://doi.org/10.1016/j.combustflame.2011.08.020
[21] Chu C, Scialabba G, Liu P, Serrano-Bayona R, Aydin FY, Pitsch H, et al. Effects of Ammonia Substitution in the Fuel Stream and Exhaust Gas Recirculation on Extinction Limits of Non-premixed Methane– and Ethylene–Air Counterflow Flames. Energy Fuels 2023;37(18):14393-403. https://pubs.acs.org/doi/10.1021/acs.energyfuels.3c02605.
[22] Chander S, Ray A. Flame impingement heat transfer: a review. Energy Conv Manag 2005;46(18-19):2803-37. https://doi.org/10.1016/j.enconman.2005.01.011
[23] Li F, Pan J, Zhang C, K. Quaye E, Shao X. Structure and Combustion Characteristics of Methane/Air Premixed Flame under the Action of Wall. Energy Eng 2021;118(4):1135-54. https://doi.org/10.32604/EE.2021.014366
[24] He C, Jiang J, Sun M, Yu Y, Liu K, Zhang B. Analysis of the NH3 blended ratio on the impinging flame structure in non-premixed CH4/NH3/air combustion. Fuel 2022;330. https://doi.org/10.1016/j.fuel.2022.125559
[25] Sun M, Jiang J, Yu Y, He C, Liu K, Zhang B. The impinging wall effect on flame dynamics and heat transfer in non-premixed jet flames. Therm Sci 2023;27(1 Part B):855-67. https://doi.org/10.2298/TSCI220126076S
[26] Wei Z, Wang L, Zhang X, Liu L, Huang G, Zhen H. Effects of flame impingement on the stability and NO/CO emissions of laminar premixed methane-ammonia impinging flame. Int J Hydrog Energy 2024;83:1078-86. https://doi.org/10.1016/j.ijhydene.2024.08.121
[27] Otsu N. A threshold selection method from gray-level histograms. Automatica 1975;11(285-296):23-7. https://doi.org/10.1109/TSMC.1979.4310076
[28] Chung SH, Law C. An invariant derivation of flame stretch. Combust Flame 1984;55(ISSN: 0010-2180). https://doi.org/10.1016/0010-2180(84)90156-1
[29] Randall JL. Finite difference methods for ordinary and partial differential equations. Philadelphia: Society for Industrial and Applied Mathematics; 2007. https://doi.org/10.1137/1.9780898717839
[30] Patankar S. Numerical heat transfer and fluid flow. Boca Raton: CRC press; 2018. https://doi.org/10.1201/9781482234213
[31] Ferziger JH, Perić M. Computational methods for fluid dynamics. Berlin, Heidelberg: Springer; 2002. https://doi.org/10.1007/978-3-642-56026-2
[32] Brown G, Roshko A. The effect of density difference on the turbulent mixing layer. Proc, AGARD Specialist Meeting on Turbulent Shear Flows; 1971.
[33] Chen L-D, Seaba J, Roquemore W, Goss L. Buoyant diffusion flames. Symposium (international) on combustion; 1989; vol. 22: Elsevier, p. 677-84.

[34] Iyogun CO, Birouk M. Effect of Fuel Nozzle Geometry on the Stability of a Turbulent Jet Methane Flame. Combust Sci Technol 2008;180(12):2186-209. https://doi.org/10.1080/00102200802414980

[35] Takahashi F, Schmoll WJ. Lifting criteria of jet diffusion flames. Symposium (International) on Combustion 1991;23(1):677-83. https://doi.org/10.1016/S0082-0784(06)80316-4

[36] Han X, Wang Z, Costa M, Sun Z, He Y, Cen K. Experimental and kinetic modeling study of laminar burning velocities of NH3/air, NH3/H2/air, NH3/CO/air and NH3/CH4/air premixed flames. Combust Flame 2019;206:214-26. https://doi.org/10.1016/j.combustflame.2019.05.003

[37] Lubrano Lavadera M, Han X, Konnov AA. Comparative effect of ammonia addition on the laminar burning velocities of methane, n-heptane, and iso-octane. Energy Fuels 2020;35(9):7156-68. https://doi.org/10.1021/acs.energyfuels.0c03424

[38] Lee B, Kim J, Chung S. Effect of dilution on the liftoff of non-premixed jet flames. Symposium (International) on Combustion 1994;25(1):1175-81. https://doi.org/10.1016/S0082-0784(06)80756-3

[39] Darabkhani HG, Wang Q, Chen L, Zhang Y. Impact of co-flow air on buoyant diffusion flames flicker. Energy Conv Manag 2011;52(8-9):2996-3003. https://doi.org/10.1016/j.enconman.2011.04.011

[40] Zhen HS, Leung CW, Cheung CS. Heat transfer characteristics of an impinging premixed annular flame jet. Appl Therm Eng 2012;36:386-92. https://doi.org/10.1016/j.applthermaleng.2011.10.053

[41] Jung KS, Kwon SH, Chung SH, Park J, Yoo CS. Flame edge dynamics in counterflow nonpremixed flames of CH4/He versus air at low strain rates: An experimental and numerical study. Combust Flame 2022;235. https://doi.org/10.1016/j.combustflame.2021.111718

[42] Cai X, Wang J, Bian Z, Zhao H, Zhang M, Huang ZJC, et al. Self-similar propagation and turbulent burning velocity of CH4/H2/air expanding flames: Effect of Lewis number. Combust Flame 2020;212:1-12. https://doi.org/10.1016/j.combustflame.2019.10.019

[43] Kohansal M, Kiani M, Masoumi S, Nourinejad S, Ashjaee M, Houshfar E. Experimental and numerical investigation of NH3/CH4 mixture combustion properties under elevated initial pressure and temperature. Energy Fuels 2023;37(14):10681-96. https://doi.org/10.1021/acs.energyfuels.3c00780

[44] Zitouni S, Brequigny P, Mounaïm-Rousselle C. Influence of hydrogen and methane addition in laminar ammonia premixed flame on burning velocity, Lewis number and Markstein length. Combust Flame 2023;253. https://doi.org/10.1016/j.combustflame.2023.112786

[45] Zhang X, Wang J, Chen Y, Li C. Effect of CH_4, Pressure, and Initial Temperature on the Laminar Flame Speed of an NH_3-Air Mixture. ACS Omega 2021;6(18):11857-68. https://doi.org/10.1021/acsomega.1c00080

[46] Hou S-S, Ko Y-C. Effects of heating height on flame appearance, temperature field and efficiency of an impinging laminar jet flame used in domestic gas stoves. Energy Conv Manag 2004;45(9-10):1583-95. https://doi.org/10.1016/j.enconman.2003.09.016

[47] Colson S, Hirano Y, Hayakawa A, Kudo T, Kobayashi H, Galizzi C, et al. Experimental and numerical study of NH3/CH4 counterflow premixed and non-premixed flames for various NH3 mixing ratios. Combust Sci Technol 2021;193(16):2872-89. https://doi.org/10.1080/00102202.2020.1763326

[48] Wang S, Elbaz AM, Wang G, Wang Z, Roberts WL. Turbulent flame speed of NH3/CH4/H2/H

2O/air-mixtures: Effects of elevated pressure and Lewis number. Combust Flame 2023;247. https://doi.org/10.1016/j.combustflame.2022.112488

[49] Wang S, Wang Z, Chen C, Elbaz AM, Sun Z, Roberts WL. Applying heat flux method to laminar burning velocity measurements of NH_3/CH_4/air at elevated pressures and kinetic modeling study. Combust Flame 2022;236:111788. https://doi.org/10.1016/j.combustflame.2021.111788

[50] Wei Z, Zhen H, Leung CW, Cheung CS, Huang Z. Heat transfer characteristics and the optimized heating distance of laminar premixed biogas-hydrogen Bunsen flame impinging on a flat surface. Int J Hydrog Energy 2015;40(45):15723-31. https://doi.org/10.1016/j.ijhydene.2015.06.047

[51] Wei Z, Zhen H, Leung CW, Cheung CS, Huang Z. Experimental and numerical study on the emission characteristics of laminar premixed biogas-hydrogen impinging flame. Fuel 2017;195:1-11. https://doi.org/10.1016/j.fuel.2017.01.056

[52] Ho C-M, Nosseir NS. Dynamics of an impinging jet. Part 1. The feedback phenomenon. J Fluid Mech 1981;105:119-42. https://doi.org/10.1017/S0022112081003133

[53] Wang Q, Huang HW, Zhang Y, Zhao C. Impinging flame ignition and propagation visualisation using Schlieren and colour-enhanced stereo imaging techniques. Fuel 2013;108:177-83. https://doi.org/10.1016/j.fuel.2013.01.048

[54] Wang Q, Zhang Y, Tang HJ, Zhu M. Visualization of diffusion flame/vortex structure and dynamics under acoustic excitation. Combust Sci Technol 2012;184(10-11):1445-55. https://doi.org/10.1080/00102202.2012.693419

[55] Phares DJ, Smedley GT, Flagan RC. The wall shear stress produced by the normal impingement of a jet on a flat surface. J Fluid Mech 2000;418:351-75. https://doi.org/10.1017/S002211200000121X

[56] Li D, Wen Y, Liu YC, Wang S. On the transition modes and mechanisms for laminar to turbulent lifted jet diffusion flames at normal-and micro-gravity. Combust Flame 2024;260:113269. https://doi.org/10.1016/j.combustflame.2023.113269

[57] Hsu C, Jhan W, Chang Y. Flow and heat transfer characteristics of a pulsed jet impinging on a flat plate. Heat Mass Transf 2020;56(1):143-60. https://doi.org/10.1007/s00231-019-02696-w

[58] Zhang F, Zirwes T, Häber T, Bockhorn H, Trimis D, Suntz R. Near wall dynamics of premixed flames. Proc Combust Inst 2021;38(2):1955-64. https://doi.org/10.1016/j.proci.2020.06.058

[59] He C, Sun M, Jiang J, Yu Y, Liu K, Zhang B. Analysis of the quenching behavior in impinging flame: Flow and thermal characteristics. Numer Heat Tranf A-Appl 2023;85(12):1973-87. https://doi.org/10.1080/10407782.2023.2214310

[60] Li H, Jiang J, Sun M, Yu Y, Sui C, Zhang BJJoT. A study of the influence of coflow on flame dynamics in impinging jet diffusion flames. 2021;22(8):461-80.

[61] Fernandes EL, RE Modeling and experimental validation of unsteady impinging flames. Combust Flame 2006;146(4):674-86. https://doi.org/10.1016/j.combustflame.2006.06.008

[62] Zhen H, Wei Z, Chen Z, Xiao M, Fu L, Huang Z. An experimental comparative study of the stabilization mechanism of biogas-hydrogen diffusion flame. Int J Hydrog Energy 2019;44(3):1988-97. https://doi.org/10.1016/j.ijhydene.2018.11.171

[63] Yang X, Ma S, Gao J, Du Q, Zhang Y, Dong H. Suppression effect prediction of mixed combustion with ammonia under sub-atmospheric pressure on flicker of methane laminar diffusion flame. Energy 2024;298:131300. https://doi.org/10.1016/j.energy.2024.131300

[64] Wimer NT, Lapointe C, Christopher JD, Nigam SP, Hayden TR, Upadhye A, et al. Scaling of the puffing Strouhal number for buoyant jets and plumes. J Fluid Mech 2020;895:A26. https://doi.o

rg/10.1017/jfm.2020.271

[65] Smith T, Menon S. Large-eddy simulations of turbulent reacting stagnation point flows. Proceedings of the 35th Aerospace Sciences Meeting and Exhibit; 1997 Jau 06-09; Reno, NV, U.S.A.: AIAA; 1997. https://doi.org/10.2514/6.1997-372

[66] Im YH, Huh KY, Kim K-YJJFE. Analysis of impinging and countercurrent stagnating flows by Reynolds stress model. J Fluids Eng 2002;124(3):706-18. https://doi.org/10.1115/1.1493815